Eur. Phys. J. B **35**, 191–199 (2003)
DOI: 10.1140/epjb/e2003-00268-2

THE EUROPEAN PHYSICAL JOURNAL B

Sample dependence of anisotropy and restriction of electron-spin diffusion in the quasi-one dimensional organic conductor (fluoranthene)$_2$PF$_6$

T. Wokrina[1], J. Gmeiner[2], N. Kaplan[3], and E. Dormann[1,a]

[1] Physikalisches Institut, Universität Karlsruhe (TH), Wolfgang-Gaede-Str. 1, 76128 Karlsruhe, Germany
[2] Bayreuther Institut für Makromolekülforschung, Universität Bayreuth, 95440 Bayreuth, Germany
[3] Racah Institute of Physics, Hebrew University of Jerusalem, 91904 Jerusalem, Israel

Received 20 May 2003

Abstract. As-grown and proton-irradiation damaged crystals of the quasi-one dimensional organic conductor (fluoranthene)$_2$PF$_6$ are studied by static magnetic field gradient spin echo electron spin resonance. The parallel-to-stack diffusion constant $D_\parallel$ varies sample dependent by a factor of 50, just like the ratio $D_\parallel/D_\perp$. The restriction of free diffusive motion of the conduction electron spins of as-grown and microstructured crystals is analyzed.

PACS. 76.30.Pk Conduction electrons – 72.15.Lh Relaxation times and mean free paths – 61.72.-y Defects and impurities in crystals, microstructure – 61.80.Jh Ion radiation effects

1 Introduction

The differentiation between charge and spin motion in one dimensional conductors is an area of current interest. Whereas treating the charge excitations in such systems is straight forward, addressing the spin motional degrees of freedom is a more subtle affair. Probably the most 'natural' technique for the study of spin-dynamics is that of Magnetic Resonance. In this context, the unique advantage of arene radical cation salts as representative model systems has been recognized shortly after their first synthesis. Due to the comparatively weak spin-orbit coupling of the radical electron spin in a pure hydrocarbon molecule, the electron spin relaxation times of organic conductors like (fluoranthene)$_2$PF$_6$ (abbreviated as (FA)$_2$PF$_6$ below) are in the range of T_1, $T_2 \approx 5 - 10$ μs even in the metallic high-temperature phase. These relatively long relaxation times enabled a study of the electron-spin dynamic properties by the same methods developed earlier in the field of nuclear magnetic resonance for phenomena that are usually slower by some five orders of magnitude. Moreover, and even more significantly, it has been directly demonstrated recently that the spin-diffusion in a related compound is completely associated with the charge-motion in the same compound [1]. We remind the reader at this point that the electronic diffusion coefficient D and the electronic mobility μ are directly related. The (FA) radical cation salts investigated here are especially appropriate candidates for a more detailed analysis, because these single crystals have sufficient long term stability, their 2:1 stoichiometry is reliably obeyed, and the experiments reported for temperatures of 250–260 K are carried out far enough from the Peierls-transition temperature ($T_P = 186$ K) that the "metallic" phase can clearly be studied.

Maresch and Mehring [2–4] have originated the study of the anisotropic motion of the charge and spin carriers in quasi-one dimensional conductors by combining the pulsed electron spin resonance (ESR) [5] with application of magnetic field gradients. For an (FA) radical cation salt, and assuming free unrestricted – but anisotropic – diffusion, they demonstrated that the techniques known from NMR (nuclear magnetic resonance) for the measurement of diffusion constants D [6,7] can be adopted for the derivation of $D(\theta)$,

$$D(\theta) = D_\parallel \cos^2\theta + D_\perp \sin^2\theta. \quad (1)$$

The quantitative analysis of $D(\theta)$ can yield in principle microscopic values of $D_\parallel$ and $D_\perp$ [4]. However in later investigations [8–12] the existence of various types of restrictions to free motion along the conducting channels in real (FA)$_2$PF$_6$ samples was demonstrated or concluded. These restrictions invalidate, at least in principle, the simple free diffusion based analysis using equation (1).

Figure 1 illustrates our current picture of real quasi-one dimensional conductors, such as the arene radical cation salts. These consist of one-dimensional stacks of aromatic hydrocarbon molecules, 'insulated' from each other by octahedral complex anions like hexafluorophosphate [13]. The electronic scattering time along the

[a] e-mail: edo@pi.uka.de

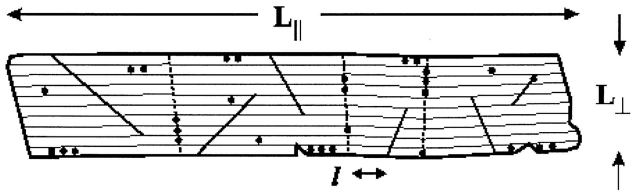

Fig. 1. Schematic view of a "real" quasi one-dimensional conducting arene radical cation salt crystal. External dimensions $(L_\parallel, L_\perp)$ and an individual channel length of free diffusive motion (l) are indicated. Grain boundaries (broken lines), cracks (solid lines) and localized defects (dots) are symbolized as the typical interruptions of the extended one-dimensional channels.

stacking direction, $\tau_\parallel$, ranges between 10^{-15} s and 10^{-14} s at room temperature, and is thus much shorter than the perpendicular hopping time, $\tau_\perp$, which is in the range of 10^{-12} s to 10^{-10} s. The anisotropy of the macroscopic microwave electrical conductivity varies, $\sigma_\parallel/\sigma_\perp = 10^3 - 10^4$, and is largely influenced by defects and mosaic structure. Cases were observed with regions in which individual channels allow for the unrestricted diffusive motion of the conduction electron spin from one end of the crystal to the other [10]. But in general there are many defects in the arene radical cation salts, and depending on the general composition and the individual growth conditions, between 10^{-5} and 10^{-2} Curie-like paramagnetic defects per formula unit exist in these systems. As illustrated in Figure 1, such defects interrupt the 1-d channels, creating finite conduction sections of length $l_\parallel$ along the channel and presumably influence $\sigma_\parallel$ – as well as the 'effective' $D_\parallel$ – in a critical manner. In fact, one would expect $\sigma_\parallel$ to be severely 'bottlenecked' by the low perpendicular conductivity as soon as enough restrictions are introduced into the sample to block effectively most of the direct conducting channels. Under such situations the charge transport and diffusion can proceed nominally only *via* the much slower perpendicular hopping rates between adjacent channels. Even for this reason alone, acquiring reliable quantitative values for $D_\perp$ and intrinsic $\sigma_\perp$ is highly desirable. Furthermore, extended obstacles – *e.g.* cracks and grain boundaries of mosaic like microstructures – that cannot be easily bypassed by the slow hopping motion perpendicular to stack in short time intervals, were also noted [13]. Such extended obstacles are presenting an additional cause for the experimentally observed monotonic increase of the absolute value of the electrical conductivity $\sigma_\parallel$ upon changing the electric field between DC (direct current) to optical frequencies.

It is clear from the above picture that important insight into the 'story' of the charge transport properties in real $(FA)_2PF_6$ samples could be gained by investigating the influence of restrictions on the electron spin diffusion in the system. The restriction to free diffusive motion of the conduction electron spins in arene radical cation salts – at least an average channel length $\bar{l}_\parallel$ – can be monitored by the static magnetic field gradient spin echo ESR technique(SGSE) [8]. Thus not only the anisotropy of spin relaxation (T_2) and spin diffusion constant ($D(\theta)$) are accessible [14,15], but also the θ-dependent influence of the restriction $\overline{l}_\parallel$ and $\overline{l}_\perp$.

The analogue of equation (1) was utilized already in an earlier preliminary study [14]. A phenomenological – or effective – average length of the conduction channels probed by the free diffusive motion, $\overline{l}(\theta)$, was derived by a numerical analysis of experimental SE-decay for magnetic field gradient in a direction θ with respect to the stacking axis. The apparent similarity of the thus derived $\overline{l}_\parallel$ values for various arene radical cation salts, ranging between 50 and 100 μm [16], was rather puzzling. The more pronounced sample dependence of the absolute values of $D_\parallel$ or of the functional dependence of $\overline{l}(\theta)$, seem to reflect the defect distribution of individual single crystals with better sensitivity. This stimulated the investigations of various individual single crystals of $(FA)_2PF_6$ reported below. The systematics of the variation of the diffusion constant $D(\theta)$ and the effective average channel length parameter $\overline{l}(\theta)$, as function of growth and aging conditions, are derived. Homogeneous and geometrically structured irradiations of single crystals with 25 MeV proton beam are used in order to probe the influence of a homogeneous and structured defect distribution on the conduction electron free diffusion.

Our specific aims in the present study: i) examine and compare the electronic spin diffusion in $(FA)_2PF_6$ samples that have been subjected to different aging and/or other relevant treatments; ii) test the utility of a specific phenomenological model calculation for the characterization of the highly anisotropic nature of the spin-diffusion in the $(FA)_2PF_6$ system; iii)try to derive reliable finite $D_\perp$ values in $(FA)_2PF_6$, for which so far only upper-limit values existed. Accordingly, the ESR experiments reported presently consist essentially of measurements of SE-decay of variety of samples as function of angle-dependent static magnetic field gradient in a direction θ with respect to the stacking axis. The observed decays were fitted by a restricted diffusion model calculation [17,18] which was modified by introducing the concept of a phenomenological, or effective, angle-dependent average channel length, $\overline{l}(\theta)$, to gain statistical robustness [14,16]. Additional – rather time consuming – fits were repeated on few selected experiments using analytic angle-depended 2-d restricted diffusion model calculation, in order to test the validy of the derived diffusion parameters. Finally, the validity of the parameters for some of the experiments was also examined by a computation-heavy 2-d random walk simulation of the anisotropic diffusion.

The paper is organized as follows. Crystal specifications, proton irradiation, pulsed ESR at 425 MHz and 9.5 GHz as well as magnetic characterization of the samples are summarized in Section 2. Modelling of the SGSE decay is explained in Section 3, including detailed random walk simulations. Our results monitoring the restrictions to free diffusion of the conduction electron spins are discussed in Section 4, considering as-grown crystals as well as crystals modified in a controled manner by homogeneous or microstructured proton irradiation. The main conclusions are summarized in Section 5.

Table 1. Sample dimensions and characteristics.

sample	$L_\parallel$(mm)	$L_\perp$(mm)	age	treatment	internal nomination
A	1.7	-	>8 y	as-grown	FA 37
B	1.61	0.23, 0.33	>8 y	as-grown	FA 326
C	1.475	0.625, 0.300	2 y	as-grown	FA 1299a
D	-	-	<1 y	as-grown	FA 0401a3
E	2.35	0.375, 0.350	<1 y	homog. irrad.	FA 0401a1
F	1.575	0.550, 0.575	<1 y	100 μm microstruct.	FA 0401a2

2 Experimental

The six different $(FA)_2PF_6$ single crystals studied in this investigation, all grown at BIMF along established electrocrystallization procedures [19], are listed and specified in Table 1. They differ in age, as given, but since they were stored in a freezer most of the time, older age does not mean longer exposure to room-temperature/humid air aging. In fact, for the oldest crystals A and B the highest purity zone-refined fluoranthene starting material was used, granting them the lowest intra stack defect content. The concentration of localized paramagnetic defects, amounting *e.g.* to 5.8×10^{-4} per formula unit for sample D (*i.e.* sample C in [20]), was further increased by the irradiation with a dose of up to 5.4×10^{16} protons (of energy $E_p=25$ MeV) per cm^2 at room temperature. This way an average defect spin concentration of 1×10^{-2} per formula unit was realized for the microstructured sample F (with periodic sequence of 100 μm-protected 100 μm-damaged segments along the stacking axis) [20].

For SGSE-instrumentation, we refer to earlier reports [8,13,14,20]. We present results obtained at $\nu_L=425$ MHz or 9.5 GHz, for magnetic field gradients up to 0.2 T m^{-1} or 1 T m^{-1}, respectively, in the 250 K–260 K temperature range. The chemical stability of the samples profits from this reduced temperature, though it is still well above the Peierls transition temperature of $T_P=186$ K of $(FA)_2PF_6$.

The data points in Figure 2 represent typical experimental SGSE decays, acquired by either the RF or the X-band ESR spectrometers from various samples, and with different magnitudes and orientations of the applied magnetic field gradient. The particular horizontal scale in the figure was chosen so as to normalize out the effects of different magnetic field gradient magnitudes for idealized free diffusion decays (see Eq. (5)). The data ranges depicted in the figure indicate also the useful dynamic range available for data analysis with each of the experiments.

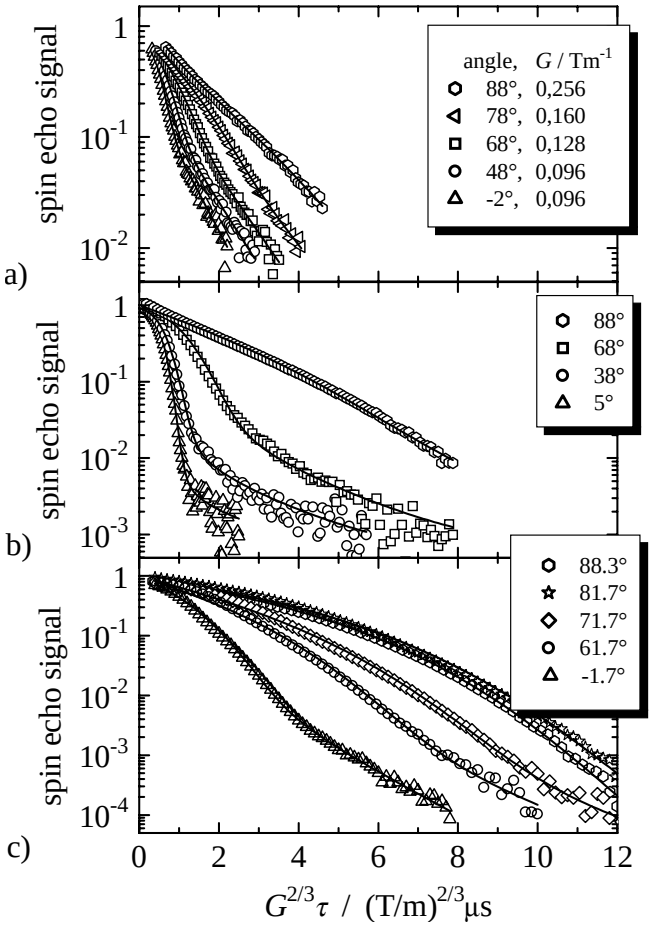

Fig. 2. Static magnetic field gradient spin echo decay (*versus* $G^{2/3}\tau$) for angles θ given in the figures. (a) Sample A, $\nu_L=425$ MHz, (b) Sample B, $\nu_L=9.5$ GHz, $G=0.93$ T m^{-1}; (c) microstructured sample F, $\nu_L=9.5$ GHz, $G=0.81$ T m^{-1}, $T=250$ K. Solid lines show fit based on equations (4) and (8).

3 Theory and data modelling

Figure 1 illustrates the possibility of a distribution of lengths $l_\parallel$ available for the free diffusive motion of the electron spins in a typical real crystal. For statistical distribution of barriers, we expect the probability

$$P(l)=\bar{l}^{-1}\exp\left(-l/\bar{l}\right) \tag{2}$$

for a segment of length l, with $\bar{l}$ defined as the average value of l. For the contribution to the normalized

SGSE-signal $M(2\tau)/M(0)$ we must convolute the characteristic echo contribution $A(l,2\tau)/A(l,0)$ of an electron spin in a channel of length l with the weight factor of spins in such channels

$$\tilde{P}(l) = l/\bar{l}^{-2}\exp\left(-l/\bar{l}\right) \tag{3}$$

i.e.

$$\frac{M(2\tau)}{M(0)} = \frac{A(l,2\tau)}{A(l,0)} \otimes \tilde{P}(l). \tag{4}$$

We note that the the simple familiar free diffusion expression [6]

$$\frac{A(2\tau)}{A(0)} = \exp\left\{-\frac{2\tau}{T_2} - \frac{2}{3}D\gamma^2G^2\tau^3\right\} \tag{5}$$

is valid for the description of the echo decay only if the free diffusion length l_D, given by

$$l_D = \langle r^2\rangle^{1/2} = (2D\cdot t)^{1/2} \tag{6}$$

is short compared to all other relevant characteristic lengths even for the longest $t = 2\tau$ values adopted in the experiment. In addition to l and l_D, it is necessary to consider also the dephasing length l_G [21,22], given by

$$l_G = (6\pi/\gamma G)^{1/3}. \tag{7}$$

Thus, the standard expression for a diffusive echo decay, equation (5), can only be used as long as $l_D \ll l_G, l$. This is then called the free diffusion limit.

3.1 Analytic limiting behavior descriptions

The so called motional narrowing regime is reached if $l \ll l_D, l_G$. Then for parallel, perfectly reflecting, non relaxing barriers with separation l, the diffusing spins average over the field variation encountered and the SGSE decay is given by [17,18]

$$\begin{aligned}\frac{A(l,2\tau)}{A(l,0)} = \exp\Bigg\{ &-\frac{2\tau}{T_2} - \frac{8\gamma^2G^2l^4}{D\pi^6}\sum_{n=0}^{\infty}\frac{1}{(2n+1)^6} \\ &\times\left[2\tau - \frac{3-4e^{-Q\tau}+e^{-2Q\tau}}{Q}\right]\Bigg\} \\ &\equiv e^{-2\tau/T_2}\times F(G^2,D,l,\tau)\end{aligned} \tag{8}$$

with $Q = D\frac{(2n+1)^2\pi^2}{l^2}$.

We note that equation (8) treats only a one-dimensional diffusion process, along the applied gradient $\boldsymbol{G}$. In actual (FA)PF_6 samples, as soon as $\boldsymbol{G}$ forms an angle θ with the direction of the conduction channels, the possible slow hopping in perpendicular direction will result in an additional independent diffusion process at right angle to the stacks. It is easy to show that in such case equation 8 should be replaced in principle by

$$\begin{aligned}\frac{A(l_\parallel,l_\perp,2\tau)}{A(l_\parallel,l_\perp,0)} = e^{-2\tau/T_2}&F({G_\parallel}^2,D_\parallel,l_\parallel,\tau) \\ &\times F({G_\perp}^2,D_\perp,l_\perp,\tau)\end{aligned} \tag{9}$$

with $G_\parallel = G\times\cos(\theta)$ and $G_\perp = G\times\sin(\theta)$

For large enough gradients [23], such that $l_G \ll l, l_D$, an edge enhancement of the signal is known to occur. If, in addition, the pulse separation τ is increased, an approximate exponential decay is derived with [21,22]

$$\frac{A(l,2\tau)}{A(l,0)} = \frac{c}{l}\left(\frac{D}{\gamma G}\right)^{1/3}\exp\left(-\frac{2\tau}{T_2} + a_1(D\gamma^2G^2)^{1/3}\tau\right) \tag{10}$$

where $c \approx 5.8841$ and $a_1 \approx -1.0188$.

All of the solid curves shown in Figure 2 are 'best fits' to the experimental data, based on the model calculation described by equations (4) and (8) alone. For each θ value, just the two parameters D and $\bar{l}$ are adjusted. This procedure defines an effective – or phenomenologic – model, physically valid only for $G(\theta)$ with $\theta = 0°, 90°$. In what follows, we call it "the effective model" for short. Compared with the generally valid 2-d model described by equation (9), the effective model reduces the fitting time while improving the fit stability, without a substantial systematic error on the relevant parameters. To explore the reliability of this procedure, random walk simulations were reanalyzed using the effective model (Eqs. (4, 8)), as described in the next section.

3.2 Random walk simulation

For purely one-dimensional random walk, the limiting cases of free diffusion, motional narrowing and localization (edge enhancement) were generated previously by a variable range hopping simulation (VRH) [13]. As a further step forward, Figure 3 shows that the result of a *two dimensional* random walk simulation can, indeed, be reasonably reproduced by a fit of the effective model. The similarity of the SGSE decays in Figures 2 and 3 is self explanatory, although the effective model fit gives $\bar{l}_\parallel = 65\,\mu$m instead of $\bar{l}_\parallel = 100\,\mu$m used for the simulation. While no deviation is observed for the diffusion parameter D, there seems to be a systematic underestimation of $\bar{l}$ when using the effective model. This was concluded already earlier from the results of spatially resolved pulsed gradient spin echo (PGSE) techniques that showed a surprising fraction of spatially unrestricted channels in $(FA)_2PF_6$ crystals, allowing free diffusion from one end of the crystal to the other [10,11].

3.2.1 Derivation of anisotropy

For the proper modelling of the SGSE decays at arbitrary orientation of $\boldsymbol{G}(\theta)$, the simple decomposition of the self diffusion coefficient D according to equation (1) is not sufficient. Rather, as alluded to in the derivation of equation (9), a model calculation based on a three-dimensional version of equations (8, 4) is required in principle. For the essentially axial treatment practiced with the present crystals, at least a convolution of equation (4) with the parallel and perpendicular diffusion attenuations, given by equation (9), is needed. This in turn requires a tedious fit of all

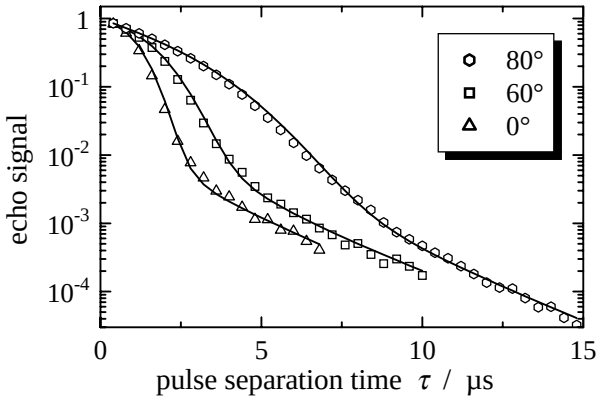

Fig. 3. Two dimensional random walk simulation of SGSE decays for various angles of $\boldsymbol{G}$. Simulations (symbols) and fits with the effective model (solid lines). Simulation parameters: Average spatial restriction of $100\,\mu$m $\times$ $10\,\mu$m; "crystal" dimensions $L_\parallel = 1$ mm; $L_\perp = 0.4$ mm; $D_\parallel = 0.2\,\mathrm{cm^2\,s^{-1}}$, $D_\perp = 2\times10^{-4}\,\mathrm{cm^2\,s^{-1}}$, $G = 1\,\mathrm{T\,m^{-1}}$, $T_2 = 5\,\mu$s. See text for further details of the effective model.

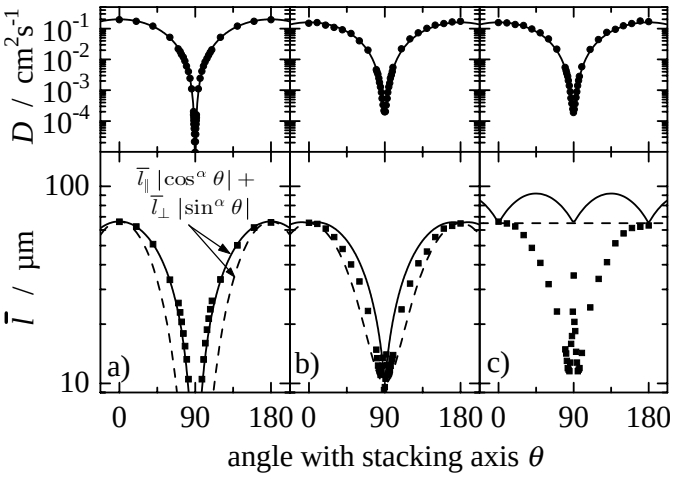

Fig. 4. Two dimensional random walk simulation of spatially restricted diffusion, reanalyzed with the effective model. See text for further details. Simulation parameters are the same as in Figure 3. For constant barrier separation of $\bar{l}_\parallel = 100\,\mu$m along the stacks, the perpendicular restriction distance was varied with $\bar{l}_\perp = 1$ Å in 4(a), $10\,\mu$m in 4(b) and $100\,\mu$m in 4(c). For $D(\theta)$, the solid line shows the fit of equation (1). For $\bar{l}(\theta)$, the calculated variation of a linear ($\alpha = 1$) and quadratic ($\alpha = 2$) superposition of $\bar{l}_\parallel$ and $\bar{l}_\perp$, *i.e.* $\bar{l}(\theta) = \bar{l}_\parallel \mid \cos^\alpha\theta \mid + \bar{l}_\perp \sin^\alpha\theta, \alpha = 1, 2$, is shown as solid and broken lines, respectively, as a guide to the eye. The $\bar{l}(\theta)$ fits for $\theta \approx 90°$ required a dynamic range of 7 orders of magnitude, unrealistic for the experimental situation depicted in Figure 2.

the angular dependent echo decays at once, considering throughout the different limiting or general descriptions referred to in Sections 3 and 3.1. In trying to avoid this difficulty, a two-dimensional random walk simulation of the echo decay was performed for realistic anisotropy of the diffusion constant $D(D_\parallel, D_\perp)$ and realistic outer dimensions of the model crystal $(L_\parallel, L_\perp)$. These numerical decay simulations were reanalyzed based on the effective model and assuming the Poisson length distribution, equations (4) and (8). Thus an *effective* average length $\bar{l}(\theta)$ was introduced, a quantity that obtains a real physical meaning only for $l_\parallel = l(\theta = 0)$ and $l_\perp = l(\theta = 90°)$. By varying the anisotropy of the individual spatial restriction – *i.e.* for constant $\bar{l}_\parallel = 100\,\mu$m, but variation of $\bar{l}_\perp$ from 1 Å over 10 μm to 100 μm (the uniform case) – the reliability of the simplified data modelling could be checked (Fig. 4). Note that Figure 4a shows the physically unrealistic situation where $\bar{l}_\perp$ restricts the diffusive motion to one molecular chain, inspite of a nonzero $D_\perp$-value.

The following conclusions can be drawn by inspection of Figure 4. In all cases the correct values of $D_\parallel$ and reasonable values of $\bar{l}_\parallel$ are obtained. If the diffusion is not restricted to one channel by the choice of very small $\bar{l}_\perp$ values, also $D_\perp$ is correctly reproduced (Figs. 4b and c). On the other hand, if the diffusion is restricted to one channel *via* use of a very small $\bar{l}_\perp$ value (Fig. 4a), we note that $\bar{l}(\theta)$ follows a $\mid \cos\theta \mid$ law. This is a clear signature of restricted 1-d diffusion, which is indeed the physical situation in the small $\bar{l}_\perp$ limit. Not unexpectedly, this situation gives rise to an overestimate of the anisotropy of the diffusion constant. The realization of this extreme situation can thus be deduced from the derived $\bar{l}(\theta)$ variation and could be used as a warning against attaching significance to $D_\perp$ values derived under such conditions.

In all other situations $\bar{l}(\theta)$ falls below the linear $\mid \cos\theta \mid$ variation (Figs 4b, c), rendering the necessary credibility to the value of $D_\perp$.

3.3 Reliability of fit parameters

In order to estimate the shortcomings of the simplified $D(\theta), \bar{l}(\theta)$ fits with the effective model, additional simulations and data modelling were performed. Figure 5a shows a few selected SGSE decays acquired from sample C. Here *all* of the SGSE decays were fitted simultaneously using the physically valid analytical 2-d model calculation based on the convolution of equation (9) with equation (3). The fitting procedure was simplified by noting that with the small expected $D_\perp$ value, the unrestricted limit ($l_\perp = \infty$) can be assumed for the perpendicular diffusion, replacing the more complicated form of $F_\perp$ with the simpler free diffusion term of equation (5). The values $D_\parallel = 0.268\ \mathrm{cm^2\,s^{-1}}, \bar{l}_\parallel = 84\ \mu\mathrm{m}, T_{2\parallel} = 2.9\ \mu$s obtained by the analytical 2-d model agree within the typical error range with the results obtained from the $D(\theta), \bar{l}(\theta)$ fits based on the effective model (see Tab. 2). The SGSE decay for $\theta = 90°$ could be described by $T_{2\perp} = 5.0\ \mu$s alone, and the value $D_\perp = 1\times10^{-6}\ \mathrm{cm^2\,s^{-1}}$ used is not really discernible from $D_\perp \equiv 0$. This poses a question mark on the reliability of the $D_\perp$-values below $6\times10^{-4}\ \mathrm{cm^2\,s^{-1}}$ given in Table 2.

Figure 5b, on the other hand, shows an attempt to fit the same experimental SGSE-decay data by assuming the observed decay signal is a superposition of two separate contributions, namely a fixed fraction "f" of localized spins, and a remaining fraction "$(1-f)$" of restricted diffusing spins. In spite of experimental indications for such

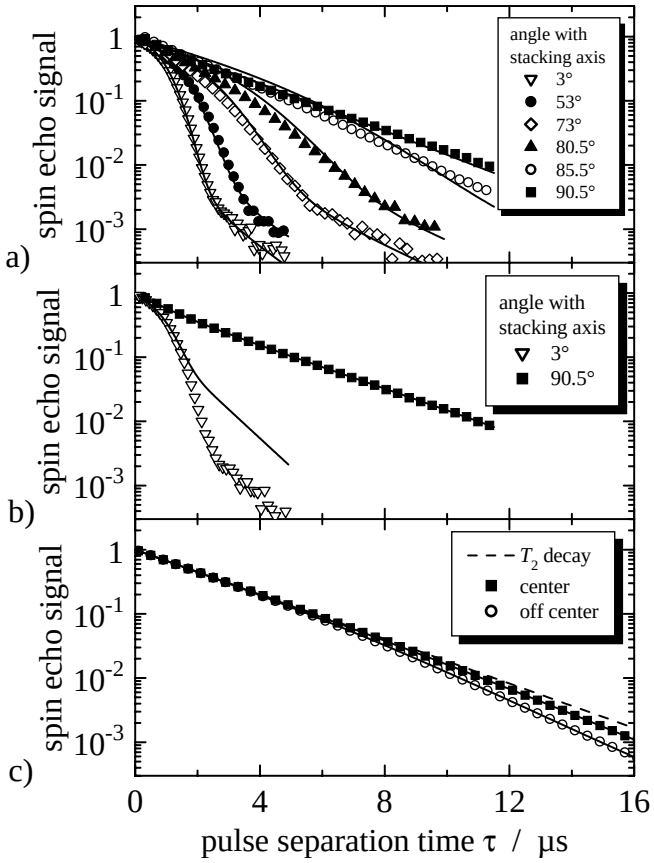

Fig. 5. Model analyses of actual SGSE decay for sample C. (a) Solid curves represent fits with a 2-d model calculation based on convolution of equation (9) with equation (3). The adjusted fit parameters: $D_\parallel = 0.268$ cm^2 s^{-1}, $\bar{l}_\parallel = 83.6$ μm, $T_{2,\parallel} = 2.9$ μs, $D_\perp = 1 \times 10^{-6}$cm^2 s^{-1}, $T_{2,\perp} = 5.0$ μs. (b) An attempt to fit the SGSE decays by a superposition of localized spins fraction and restricted diffusing spins fraction, f and $(1-f)$, respectively, with $f = 0.339$ and $T_{2,l} = 1.93$ μs. For the delocalized spins: $T_{2,\parallel} = 3.08$ μs, $D_\parallel = 0.264$ cm^2 s^{-1}, ($\bar{l}_\parallel = 200$ μm), $T_{2,\perp} = 5.37$ μs, ($D_\perp = 2.0 \times 10^{-5}$ cm^2 s^{-1}, $l_\perp = \infty$). (c) The points are calculated SGSE decay values for $\theta = 90°$, $D_\perp = 0$, $T_2 = 5.0$ μs, influenced by the spurious transversal gradient G_y and assumed $D_\parallel = 0.229$ cm^2 s^{-1}, for sample C in center or off-center position. The solid curves represent analysis of these data by the effective model, 'predicting' $D_\perp = 1.2 \times 10^{-4}$ cm^2 s^{-1} (5.1×10^{-4} cm^2 s^{-1}) and $l_\perp = 1.1$ μm (1.7 μm) for center (off center) position, respectively. The broken line shows the single exponential T_2 decay.

localized spins [8,20], this type of decomposition fails evidently in Figure 5b for the $\theta \approx 0°$ orientation. Again, the correct $D_\parallel$-value is found, however.

Finally, in Figure 5c we analyse the possible influence a small spurious magnetic field gradient component in the direction y perpendicular to the main gradient direction z (G_z is parallel to the resonance field B_z). Indeed, a curvature of the computed echo decay shown in the semilogarithmic plot is observed inspite of $D_\perp$ being assumed to be identically zero. For the iron wedges used in our X-band (9.5 GHz) system this gradient component G_y is zero in the central sample position, but grows linearly by about 0.038 (T m^{-1})mm^{-1} for off-center positions (for a main gradient $G_z = 0.49$ T m^{-1}) [24]. Thus the calculated SGSE decay for the crystal's needle axis oriented at $\theta = 90°$ is influenced by $D_\parallel$, nevertheless, and in spite of the $D_\perp \equiv 0$, the calculated SGSE decay suggests a finite apparent value of $D_\perp$. In Figure 5c we compare the effect for an exactly centered crystal C ($L_\parallel$ see Tab. 1) and for an extremal situation, where one end of the crystal C just reaches this central position. Reanalysing these simulated data with the effective model, and for $D_\parallel = 0.229$ cm^2 s^{-1}, $T_2 = 5$ μs appropriate for crystal C, we derive "apparent" values $D_\perp = 1.2{\times}10^{-4}$ cm^2 s^{-1} ($5.1{\times}10^{-4}$ cm^2 s^{-1}), $\bar{l}_\perp = 1.1$ μm (1.7 μm) and anisotropies $D_\parallel/D_\perp = 1860$ (450) for centered (off-center) position.

Thus, we must conclude that the maximum $D_\parallel/D_\perp$-anisotropy is instrumentally limited to about 2000 for our X-band set-up at present. The extension of the $D_\perp$-minimum limit for crystals with large $D_\parallel$ values requires an even better control of the spurious G_x and G_y gradients than is currently achievable in our X-band system.

4 Discussion of the results

4.1 As-grown crystals

Figure 6 shows the derived diffusion parameter D for three as-grown $(FA)_2PF_6$ crystals (A, B, C). A sample dependent variation of the diffusion constant $D_\parallel$ by a factor of almost 20 is observed (Tab. 2). The restriction to free diffusion for this direction is sample dependent as well, but to a much smaller extend. The averaged value $\bar{l}_\parallel$ varies less than a factor of two, and is not simply correlated with the $D_\parallel$ values. This is in line with the reasoning presented earlier [14] that individual intra-stack defects reduce the effective diffusion constant, but due to the possibility of hopping to a neighboring stack, spatial restriction requires extended obstacles that can not be bypassed in the microsecond time scale. For sample A with the strongest anisotropy of the diffusion constant, and the smallest estimated $D_\perp$ value, obstacles seem less easy to circumvent. On the other hand, according to the rules derived *via* the random walk simulations, Section 3.2.1, the ratio $D_\parallel/D_\perp \geq 3.4 \times 10^4$ collected in Table 2 for sample A is suspected to overestimate the anisotropy on account of the fact that the limiting $\bar{l}(\theta)$-variation (*i.e.* $\alpha = 1$ as in Fig. 4a) was derived in this case.

4.2 Homogeneously damaged crystal

Analysing $\theta = 0$ X-band SGSE decays from the homogeneously proton irradiated sample E with the effective model, the diffusion constant $D_\parallel = 0.093$ cm^2 s^{-1} and the average barrier separation $\bar{l}_\parallel = 17$ μm are obtained. The anisotropy of the diffusion constant derived at 450 MHz (Fig. 7) is reduced to about two orders of magnitude only (Tab. 2). Here, the more pronounced restriction of the conduction electron spin diffusion in the stacking direction ($\bar{l}_\parallel$) is behaving similar to the reduction of the intra-stack diffusion constant $D_\parallel$.

Table 2. Diffusion constants of $(FA)_2PF_6$ samples.

Sample	T(K)	$D_\parallel$(cm^2 s^{-1})	$\bar{l}_\parallel(\mu m)$	$D_\perp$(cm^2 s^{-1})	$D_\parallel/D_\perp$	$\tau_\perp$(s)
A	260	4.00 ± 0.09	88 ± 9	$(\leq 1.15 \times 10^{-4})$	$(\geq 3.4 \times 10^4)$	$(\geq 1.6 \times 10^{-10})$
B	260	1.9 ± 0.1	165 ± 14	$\leq 1 \times 10^{-3}$	≥ 1900	$\geq 1.9 \times 10^{-11}$
C	250	0.225 ± 0.003	98 ± 1	$\leq 6 \times 10^{-4}$	≥ 380	$\geq 3.1 \times 10^{-11}$
E	250	0.081 ± 0.001	17 ± 2	$(6.8 \pm 0.5) \times 10^{-4}$	≈ 120	$\approx 2.7 \times 10^{-11}$
F	250	0.071 ± 0.001	20 ± 2	$(1.0 \pm 0.5) \times 10^{-3}$	≈ 70	$\approx 1.9 \times 10^{-11}$

(According to the criteria derived in 3.2.1, the value of $D_\perp$ for sample A could also be underestimated.)

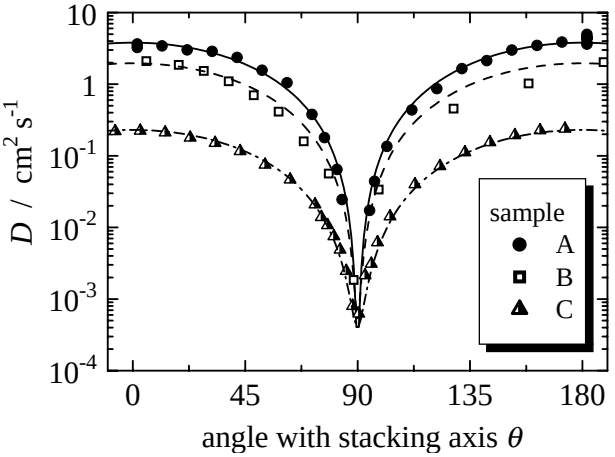

Fig. 6. Diffusion constant $D(\theta)$ derived with help of the effective model for samples A, B, C. Experimental conditions (A): $T = 260\,\mathrm{K}$, $\nu_L = 425\,\mathrm{MHz}$, $G = 0.064$ ...$0.224\,\mathrm{T\,m^{-1}}$; (B): $T = 260\,\mathrm{K}$, $\nu_L = 9.5\,\mathrm{GHz}$, $G = 0.930\,\mathrm{T\,m^{-1}}$; (C): $T = 250\,\mathrm{K}$, $\nu_L = 9.5\,\mathrm{GHz}$, $G = 0.923\,\mathrm{Tm^{-1}}$. $D_\parallel$-, $D_\perp$-values: see Table 2. $\bar{l}_\parallel, \bar{l}_\perp$: (88 ± 9) μm, ≤ 2 μm, (A); (165 ± 14) μm, (10 ± 5) μm, (B); (98 ± 1) μm, ≤ 0.6 μm, (C).

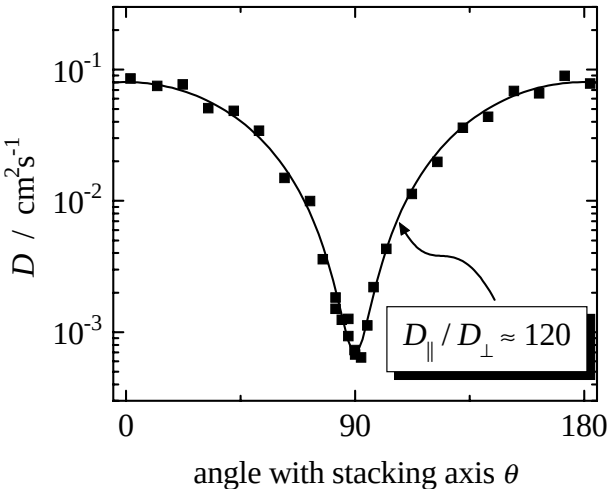

Fig. 7. Orientation dependence of the diffusion constant, $D(\theta)$, in the homogeneously irradiated sample E. ($T = 250\,\mathrm{K}$, $\nu_L = 450\,\mathrm{MHz}$). For the fit parameters see Table 2.

4.3 Microstructured crystal

Single crystal F was microstructured by irradiation with a high energy (25 MeV) proton beam *via* a masking grid presenting an alternating array of 100 μm wide open and closed stripes [20]. Nevertheless, spin diffusion in magnetic field gradient oriented at an angle θ with respect to the stacking axis gives rise to a SGSE decay that can be reasonably analyzed based on the same models as for the homogeneous crystals. Figure 8 shows the results for $\bar{D}(\theta)$, which are now average values for both damaged and undamaged regions, and thus averaged not only over the "standard" distribution. The reduction of the derived value of $\bar{D}_\parallel$ and the ratio $\bar{D}_\parallel/\bar{D}_\perp$ comes close to the results derived for the homogeneously irradiated sample E. Thus we conclude that the damaged areas of the $(FA)_2PF_6$ crystal F predominate in the measured SGSE decay. Evidently the radiation damage reduces the parallel-to-stack diffusion and thus also the corresponding echo attenuation [20].

The effective value of the average restriction, $\bar{l}(\theta)$, turns out to be isotropic and amounts to about 20 μm, five times smaller than the value appropriate for $\bar{l}_\parallel$ of as-grown crystals. This may be compared with the geometrical size of irradiated and non-irradiated blocks of 100 μm.

5 Conclusions

Barriers in the conducting chain are of particular importance for the properties of quasi-one dimensional conductors. They reduce the direct current electrical conductivity and give rise to a frequency dependence of the conductivity, they are responsible to a large extent for the angular and temperature dependence of ESR line-width and relaxation, and eventually, if they break the one-dimensional stacks into short enough segments, they can even suppress the Peierls transition typically expected as a consequence of electron phonon interaction [25]. The influence of such barriers on the anisotropy and the spatial restriction of conduction electron spin free diffusion is investigated here, analysing as-grown and artificially damaged radical cation salt crystals. As an especially appropriate model system for this kind of analysis, the $(\text{fluoranthene})_2PF_6$ radical

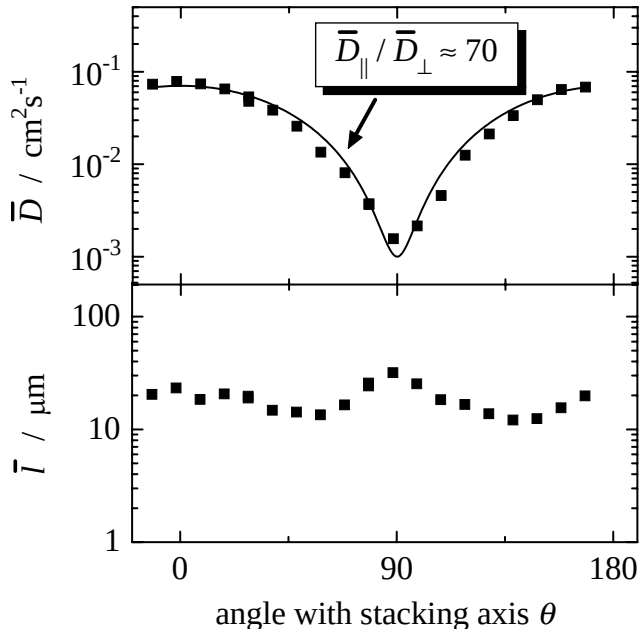

Fig. 8. Orientation dependence of $\bar{D}(\theta)$ and $\bar{l}(\theta)$ for the microstructured sample F (average values for damaged as well as undamaged regions). ($T = 250\,\mathrm{K}$, $\nu_L = 9.5$ GHz, $G = 0.81\ \mathrm{Tm}^{-1}$).

cation salt is adopted in its metallic high temperature phase. Transverse relaxation times $T_2 \geq 5\ \mu$s and conductivity as well as spin diffusion anisotropies of above 10^3:1, combined with reasonable long term stability of the crystals, distinguish these crystals. In addition, like for all organic material, proton irradiation can be used to modify the barrier properties, either uniformly or in a structured manner.

We used the method of static gradient spin echo ESR for the derivation of the absolute value and the anisotropy of the diffusion constant $D(\theta)$. Random walk simulations verified that the geometry of the restriction of free diffusion along the preferred direction can be reasonably determined as well, but the comparatively small diffusion constant in the perpendicular direction, $D_\perp$, prevents a reliable probing of possible restrictions in this direction. Thus the primary information source on the extension of defects is the comparison of their effect on the absolute value $D_\parallel$ and on the spatial restriction of stack-parallel motion, $\bar{l}_\parallel$, because the latter identifies obstacles that are so large that they can not be bypassed within the time scale of the experiment.

One of the $(FA)_2PF_6$ crystals analyzed above shows a very large spin diffusion constant $D_\parallel = 4.0\ \mathrm{cm}^2\,\mathrm{s}^{-1}$ (sample A). This same crystal was analyzed in a spatially resolving pulsed gradient spin echo experiment [10], and showed regions where the free diffusion is restricted only by the actual crystal dimensions. For the other as-grown crystals (B, C) a $D_\parallel$-variation by a factor of 20 was found. Further reduction of $D_\parallel$ by proton irradiation was achieved for the two other samples (E and F). Thus spin diffusion analysed on the microsecond time scale is sample dependent as well as amenable to arbitrary manipulation in $(FA)_2PF_6$ crystals.

Semi-quantitative information on the spatial restriction of free diffusion can be extracted from SGSE analysis. It is expressed by the average length $\bar{l}_\parallel$ of an exponential channel length distribution function. This quantity shows again a sample dependence, that is not directly correlated with the variation of $D_\parallel$, however. The curious constancy of $\bar{l}_\parallel$ values reported earlier – all fall in the 50–150 μm range – probably mainly reflects the typical quality of arene radical cation salts grown by electrochemical techniques. It is supporting a physical interpretation, however, that $\bar{l}_\parallel$-values could be reduced by a factor of five (to the $\bar{l}_\parallel \approx 20\ \mu$m range) *via* proton-irradiation created defects in the course of this investigation.

The diffusion constant for motion of the spins perpendicular to the stacking direction is small and typically resides at or below the detection limit. Thus access to a $D_\perp$-limiting value can best be based on the analytical description of the $D(\theta)$ variation by equation (1). Our simulations indicate, however, that the anisotropy actually can also be overestimated this way. The mechanism responsible for the perpendicular diffusion constant $D_\perp$ is currently still unclear. Thus the experimental comparison of spin and charge motion perpendicular to the stacking direction is still a duty of forthcoming experiments.

It is clearly shown by the experimental results and the modelling of the SGSE decay of radiation damaged in comparison to various as-grown $(FA)_2PF_6$ crystals that the anistropy of the conduction electron spin diffusion constant, $D(\theta)$, can be reduced in a controlled manner from values considerably above 1000 to values even below 100 in this model system of quasi-one dimensional conductors.

We are indebted to G. Alexandrowicz, A. Feintuch, J.U. von Schütz and T. Tashma for discussions and M. Drescher and B. Pongs for experimental contributions. We thank P. Höfer and Bruker/Karlsruhe for the opportunity to perform early pulsed ESR measurements at 10 GHz. One of us (N.K.) acknowledges with thanks a guest professorship accorded by the Deutsche Forschungsgemeinschaft /GK 284 (Universität Karlsruhe), and partial research support by the Israel Science Foundation (grant 28/01). This project is supported by the DFG (Do 181/10).

References

1. T. Tashma, G. Alexandrowicz, N. Kaplan, E. Dormann, A. Grayevsky, A. Gabay, Synth. Metals **106**, 151 (1999)
2. G.G. Maresch, A. Grupp, M. Mehring, J.U. von Schütz, H.C. Wolf, J. Phys. France **46**, 461 (1985)
3. G.G. Maresch, *Zeitaufgelöste Elektronenspinresonanz zur Untersuchung von Elektron-Spindiffusion mit und ohne Elektronentransport in organischen eindimensionalen Leitern,* Ph.D. thesis, Universität Stuttgart, Germany, 1987
4. M. Mehring in: *Low-Dimensional Conductors and Superconductors*, edited by D. Jérome, L.G. Caron (Plenum Publishing Corp., 1987), p. 185

5. G. Sachs, W. Stöcklein, B. Bail, E. Dormann, M. Schwoerer, Chem. Phys. Lett. **89**, 179 (1982)
6. H.C. Torrey, Phys. Rev **104**, 563 (1956)
7. J.E. Tanner, E.O. Stejskal, J. Chem. Phys. **49**, 1768 (1968)
8. R. Ruf, N. Kaplan, E. Dormann, Phys. Rev. Lett. **74**, 2122 (1995); **75**, 1237 (1995); **76**, 334 (1996)
9. N. Kaplan, E. Dormann, R. Ruf, A. Coy, P.T. Callaghan, Phys. Rev. B **52**, 16385 (1995)
10. G. Alexandrowicz, T. Tashma, A. Feintuch, A. Grayevsky, E. Dormann, N. Kaplan, Phys. Rev. Lett. **84**, 2973 (2000)
11. T. Tashma, A. Feintuch, A. Grayevsky, J. Gmeiner, A. Gabay, E. Dormann, N. Kaplan, Synth. Metals **132**, 161 (2003)
12. A. Feintuch, T. Tashma, A. Grayevsky, J. Gmeiner, E. Dormann, N. Kaplan, J. Magn. Res. **157**, 69 (2002)
13. T. Wokrina, *Räumlich eingeschränkte Elektronen-Spindiffusion in quasi-eindimensionalen organischen Leitern*, Ph.D. thesis, Universität Karlsruhe, Germany (2002) (Shaker-Verlag, Aachen, 2002)
14. T. Wokrina, E. Dormann, N. Kaplan, Europhys. Lett. **49**, 244 (2000)
15. T. Wokrina, E. Dormann, J. Gmeiner, Synth. Metals **120**, 847 (2001)
16. T. Wokrina, E. Dormann, N. Kaplan, Phys. Rev. B **54**, 10492 (1996)
17. C.H. Neumann, J. Chem. Phys. **60**, 4508 (1974)
18. B. Robertson, Phys. Rev. **151**, 273 (1966)
19. V. Enkelmann, Adv. Chem. Ser. **217**, 177 (1988)
20. T. Wokrina, J. Gmeiner, N. Kaplan, E. Dormann, Phys. Rev. B **67**, 054103 (2003)
21. M.D. Hürlimann, K.G. Helmer, T.M. de Swiet, P.N. Sen, C.H. Sotak, J. Magn. Res. A **113**, 260 (1995)
22. T.M. de Swiet, P.N. Sen, J. Chem. Phys. **100**, 5597 (1994)
23. P.T. Callaghan, *Principles of Nuclear Magnetic Resonance Microscopy* (Oxford Science Publications, Oxford, 1995)
24. M. Drescher, private communication
25. I. Baldea, H. Köppel, L.S. Cederbaum, J. Phys. Soc. Jpn **68**, 1954 (1999)